

Predicting aerodynamic characteristics of airfoils using artificial neural network

Md. Moynul Hasan

moynul0210@gmail.com

Bangladesh University of Engineering and Technology

Mohammad Fahim Faisal

Bangladesh University of Engineering and Technology

N.M. Golam Zakaria

Bangladesh University of Engineering and Technology

Md. Mashiur Rahaman

Bangladesh University of Engineering and Technology

Research Article

Keywords: Airfoil, Wind turbine, Computational fluid dynamics, Lift coefficient, Drag coefficient, Artificial neural network

Posted Date: March 26th, 2024

DOI: <https://doi.org/10.21203/rs.3.rs-4156906/v1>

License:  This work is licensed under a Creative Commons Attribution 4.0 International License.

[Read Full License](#)

Additional Declarations: The authors declare no competing interests.

Predicting aerodynamic characteristics of airfoils using artificial neural network

Md. Moynul Hasan, Mohammad Fahim Faisal, N.M. Golam Zakaria, and Md. Mashiur Rahaman

ABSTRACT

In this study, an artificial neural network (ANN)-based method is proposed to predict the aerodynamic characteristics of airfoils, such as NACA 0012, NACA 0015, NACA 0018, NACA 0021, and NACA 0025, approximating the flow around airfoils as a function of the Reynolds number (Re), angle of attack (α), airfoil coordinates (X, Y), and predicting the lift coefficient (C_L) and drag coefficient (C_D) without using extensive software packages. Wind turbine data were obtained for C_L and C_D for different α ($0^\circ \leq \alpha \leq 180^\circ$) and different values of Re ($10^4 \leq Re \leq 10^7$). An ANN model was trained to achieve a root mean square error (RMSE) of less than 0.12 and 0.025 for C_L and C_D , respectively. For C_L and C_D , the RMSE of the trained model used to evaluate the new data was less than 0.09 and 0.12, respectively. Subsequently, the results were validated in a two dimensional numerical domain using RANS-CFD simulations and experimental data, showing that the proposed ANN approach is in good agreement for predicting the stall shape and aerodynamic characteristics at an angle of attack (α) ranging from ($0^\circ \leq \alpha \leq 30^\circ$).

INTRODUCTION

Analysis of flow past airfoils has many practical applications in aerodynamics (Ismail et al. 2015; Singh et al. 2022; Gao et al. 2017) and hydrodynamics (Guo et al. 2019; Karim et al. 2014; Sener and Aksu 2022), such as the design of air vehicles, wind turbines, fans, rudders, and aircraft (Lin et al. 2013). The airfoil shape is responsible for producing lift and drag for

wind turbines, aircraft wings, and ship rudders. Therefore, the precision of the lift coefficient (C_L) and drag coefficient (C_D) has a significant impact on the airfoil design process. The NACA series is the most widely used airfoil profile owing to its unique geometry, which allows for a high lift and low drag, making it both economical and effective. This unique geometry also contributes to the airfoil strength and stall reduction. NACA profiles are also used in other foil-shaped structures, such as propellers (Takekoshi et al. 2005), propeller ducts (Yilmaz et al. 2013), marine current turbines (Goundar et al. 2012), and fins (Ram et al. 2015). Furthermore, owing to its extensive application in various fields of study, the NACA series is the most thoroughly investigated airfoils. The standard NACA 00 series is used in various ships (Liu et al. 2016), wind turbines (Douvi and Margaris 2012), and aircraft wings (Del Pino et al. 2011). Currently, the majority of this flow analysis is performed using computational fluid dynamics (CFD), which solves the Navier–Stokes (NS) equations (Rojas-Sola et al. 2016). However, there are a few drawbacks in using CFD for flow analysis. For example, the CFD solution accuracy is highly dependent on the initial or boundary conditions used as an input to the numerical model (Raman et al. 2018). Furthermore, the high cost of CFD analysis is primarily owing to the need for very high computational power (Jameson 1996) and the time required to generate many accurate aerodynamic databases (Tang et al. 2005).

Trained artificial neural network (ANN) models have recently gained attention for learning the responses of large, complex, and nonlinear systems (Liu et al. 2017). This trend has spread to physical modeling simulations, wherein traditional techniques are being replaced by deep learning, or more specifically, ANNs (Kononenko and Kononenko 2018; Jokar and Semperlotti 2021). A variety of deep learning approaches are being used to simplify the novel numerical computations associated with flow analysis because a trained neural network can produce results in near real time compared to CFD analysis. (Guo et al. 2016) used a convolutional neural network (CNN) to analyze non-uniform steady laminar flow fields around bluff body objects. (Lee and You 2019) used deep learning to predict unsteady flow fields

over a circular cylinder based on the data. For fluid flow problems, (Cai et al. 2022; Mao et al. 2020; Sekar et al. 2022; Bai and Zhang 2022) used physics-informed neural networks (PINNs) (Raissi et al. 2019).

In analyzing the flow past an airfoil, (Bhatnagar et al. 2019) used a CNN to predict the velocity and pressure distributions around an airfoil. In contrast, different CNN architectures and training methods have been combined to compute aerodynamic coefficients such as the lift, drag, and pitch moment coefficient of a flow past an airfoil (Chen et al. 2020; Yuan et al. 2018; Zhang et al. 2018). (Sekar et al. 2019) used a combination of CNNs and a multilayer perceptron (MLP) to predict the flow around airfoils. (Yu et al. 2019) developed a more complex CNN architecture than their peers to predict the lift coefficient better. (Xu et al. 2021) predicted unsteady cavitation around a Clark-Y hydrofoil by using machine learning. Finally, (Peng et al. 2022) used an element spatial convolution neural network (ESCNN) for predicting the airfoil lift coefficient (C_L).

Because problems must be converted into numerical values before being introduced into an ANN, a dataset of various aerodynamic coefficients must be generated to train the neural network. The dataset can be derived from the NS equation-based CFD simulations, wind tunnel test measurements, or a combination of these (Thirumalainambi and Bardina 2003). Previous studies that used ANN models to predict aerodynamic characteristics relied heavily on different CFD simulation software tools to generate training data (Zhang et al. 2018; Ahmed et al. 2022; Oztiryaki and Piskin 2021; Bhatnagar et al. 2019; Sekar et al. 2019; Peng et al. 2022). However, CFD simulation software tools have certain real-world limitations, most notably, the inability to accurately predict the stall angle when compared to experimental data (Suvanjumrat 2017; Kallstrom). Consequently, ANN models generated from these data will eventually mimic those limitations because the accuracy of the ANN is heavily dependent on the data quality during the training phase. The dataset used in this study was obtained from the results of a wind-turbine experiment (Sheldahl and Klimas 1981). This study aims to use an ANN to predict the aerodynamic characteristics of airfoils

accurately.

RANS-BASED CFD ANALYSIS

Numerical simulations of the NACA 0012 (Douvi et al. 2012), NACA 0015 (Şahin and Acir 2015), NACA 0018 (Timmer 2008), NACA 0021 (Holst et al. 2018), and NACA 0025 (Castelli et al. 2012), which are part of a family of NACA 4-digit symmetric airfoils, were performed. Such airfoils are used in marine rudders (Tasif et al. 2017; Liu et al. 2016), marine turbines (Consul et al. 2013), and wind turbines (Claessens 2006; Mohamed 2012). The simulations were performed using ANSYS Fluent Students version 2022, and ANSYS Mechanical Students version 2022 was used to generate high-quality meshes.

Mathematical Formulation

The equation for mass conservation and momentum conservation for any fluid flow problem can be written as (Douvi et al. 2012)

$$\frac{\partial \rho}{\partial t} + \nabla \cdot (\rho \vec{u}) = S_m, \quad (1)$$

$$\frac{\partial}{\partial t}(\rho \vec{u}) + \nabla \cdot (\rho \vec{u} \vec{u}) = -\nabla p + \nabla \cdot (\bar{\tau}) + \rho \vec{g} + \vec{F}, \quad (2)$$

where $\bar{\tau}$ is the stress tensor, which can be written as

$$\bar{\tau} = \mu \left[(\nabla \vec{u} + \nabla \vec{u}^T) - \frac{2}{3} \right] \nabla \cdot \vec{u} I. \quad (3)$$

For two-dimensional (2-D) steady and incompressible flows, the continuity equation and momentum equations for viscous flow in the x and y directions can be expressed as follows:

$$\frac{\partial u}{\partial x} + \frac{\partial v}{\partial y} = 0, \quad (4)$$

$$\rho \frac{Du}{Dt} = -\frac{\partial p}{\partial x} + \frac{\partial \tau_{xx}}{\partial x} + \frac{\partial \tau_{yx}}{\partial y} + \rho f_x, \quad (5)$$

$$\rho \frac{Dv}{Dt} = -\frac{\partial p}{\partial y} + \frac{\partial \tau_{xy}}{\partial x} + \frac{\partial \tau_{yy}}{\partial y} + \rho f_y. \quad (6)$$

Turbulence Models

Simulations were performed using realizable $k-\epsilon$ (Shih et al. 1995), $k-\omega$ SST (Menter 1994), and the Spalart–Allmaras turbulence model (Spalart and Allmaras 1992) with a Reynolds number (Re) of 1.6×10^5 and an angle of attack (α) ranging from 0° to 30° .

Realizable $k - \epsilon$ Model

The realizable $k - \epsilon$ model predicted the planar and round jet spreading rates more accurately. It could also perform well in rotational flows and boundary layers with high-pressure gradients, separation, and recirculation (Bulat and Bulat 2013). The transport equations in this model are as follows (Douvi et al. 2012):

$$\frac{\partial}{\partial t}(\rho k) + \frac{\partial}{\partial x_j}(\rho k u_j) = \frac{\partial}{\partial x_j} \left[\left(\mu + \frac{\mu_t}{\sigma_k} \right) \frac{\partial k}{\partial x_j} \right] + G_k + G_b - \rho \epsilon - Y_u + S_k, \quad (7)$$

$$\frac{\partial}{\partial t}(\rho \epsilon) + \frac{\partial}{\partial x_j}(\rho \epsilon u_j) = \frac{\partial}{\partial x_j} \left[\left(\mu + \frac{\mu_t}{\sigma_\epsilon} \right) \frac{\partial \epsilon}{\partial x_j} \right] + \rho C_1 S \epsilon - \rho C_2 \frac{\epsilon^2}{k + \sqrt{v \epsilon}} + C_{1\epsilon} \frac{\epsilon}{k} C_{3\epsilon} G_b + S_\epsilon, \quad (8)$$

where

$$C_1 = \max \left[0.43, \frac{n}{n+5} \right], n = S \frac{k}{\epsilon}, S = \sqrt{2S_{ij}S_{ij}}. \quad (9)$$

The formation of turbulent kinetic energy due to the mean velocity gradients is represented by G_k in these equations. The formation of turbulent kinetic energy owing to buoyancy is denoted by G_b , and Y_M indicates the contribution of variable dilatation to the overall dissipation rate in compressible turbulence ($Y_M = 2\rho\epsilon M_t^2$, where M_t is the turbulent Mach number). The turbulent Prandtl numbers for k and ϵ are σ_k and σ_ϵ , respectively. The source terms S_k and S_ϵ are user defined. The realizable $k - \epsilon$ model constants are $C_{1\epsilon}=1.44$, $C_2 = 1.9$, $\sigma_k = 1$, and $\sigma_\epsilon = 1.2$.

SST $k - \omega$ Model

The SST $k - \omega$ turbulence model, which is suitable for industrial applications, combines the standard $k - \epsilon$ model in free flow with the Wilcox $k - \omega$ model near walls. It has the same resolution requirements as the Wilcox $k - \omega$ model and low Reynolds number as the standard $k - \epsilon$ model; however, its formulation eliminates some of the shortcomings of these models (Versteeg and Malalasekera 2007; Frei 2017). The $k - \omega$ SST model has two equations that can be written as (Suvanjumrat 2017)

$$\frac{\partial(\rho k)}{\partial t} + \operatorname{div}(\rho k U_i) = \operatorname{div} \left[\left(\mu + \frac{\rho k}{\omega \sigma_k} \right) \nabla k \right] + 2 \frac{\rho k}{\omega} S_{ij} \cdot S_{ij} - \frac{2}{3} \rho k \frac{\partial U_i}{\partial x_j} \delta_{ij} - \beta^* \rho k \omega, \quad (10)$$

$$\frac{\partial(\rho \omega)}{\partial t} + \operatorname{div}(\rho \omega U_i) = \operatorname{div} \left[\left(\mu + \frac{\rho k}{\omega \sigma_{\omega 1}} \right) \nabla \omega \right] + 2 \rho \gamma_2 S_{ij} \cdot S_{ij} - \frac{2}{3} \rho \gamma_2 \omega \frac{\partial U_i}{\partial x_j} \delta_{ij} - \beta_2 \rho \omega^2 + 2 \frac{\rho}{\omega \sigma_{\omega 2}} \frac{\partial k}{\partial x_k} \frac{\partial \omega}{\partial x_k}, \quad (11)$$

where k , ω , ν , and y represent the turbulent kinematic energy, turbulent frequency, dynamic viscosity, and distance to the solid wall, respectively, and σ_k , β^* , $\sigma_{\omega 1}$, γ_2 , β_2 , and $\sigma_{\omega 2}$ have values of 1.0, 0.09, 2.0, 0.44, 0.083, and 1.17, respectively.

Spalart–Allmaras Model

The Spalart–Allmaras model is an airfoil-applicable, one-equation turbulence model. The model is effective at predicting stalled flows in boundary layers with adverse pressure gradients (Versteeg and Malalasekera 2007). The equation for this model can be written as (Suvanjumrat 2017)

$$\frac{\partial(\rho\tilde{v})}{\partial t} + \operatorname{div}(\rho\tilde{v}U_i) = \frac{1}{\sigma_v} \operatorname{div} \left[(\mu + \rho\tilde{v})\nabla\tilde{v} + \rho C_{b2} \frac{\partial\tilde{v}}{\partial x_i} \frac{\partial\tilde{v}}{\partial x_i} \right] + \rho C_{b1} \tilde{v} \tilde{\Omega} - \rho C_{w1} \left(\frac{\tilde{v}}{\kappa y} \right)^2 f_w, \quad (12)$$

$$\tilde{\Omega} = \Omega_{ij} + \frac{\nabla}{(\kappa y)^2} f_{v2}, \quad (13)$$

where \tilde{v} , $\tilde{\Omega}$, Ω_{ij} , and μ represent the kinematic eddy viscosity, local mean vorticity, and mean vorticity tensor, respectively. Furthermore, the wall-damping functions are denoted as $f_{v2} = f_{v2}(\tilde{v}/v)$ and f_w . The values of σ_v , C_{b1} , C_{b2} , and k are 0.67, 0.1355, 0.622, and 0.4187, respectively.

Airfoil Domain and Boundary Conditions

(Suvanjumrat 2017) studied the effects of domain dimensions on the RANS-CFD solution accuracy and found that the average error of the lift and drag coefficients for a downstream length of 26 times the chord length of the airfoil was less than that of other varied downstream lengths for the NACA 0015 airfoil. Therefore, a C-type domain with a radius of 13c and downstream length of 26c was used, as shown in Fig. 1.

Uniform velocities were assigned to the inlet flow on the left side of the C-type domain. The top and bottom walls are subjected to slip boundary conditions. Atmospheric pressure controlled the right side of the domain outlet flow. The symmetry form of the boundary condition defined the front and rear domains. No-slip conditions ($u_p = 0$) were imposed only on the airfoil profile wall. For the simulations, the Reynolds number (Re) was 1.6×10^5 , indicating that the flow was incompressible. Consequently, an incompressible flow of air with a density (ρ) of 1.225 kg/m^3 and a dynamic viscosity (ν) of $1.7894 \times 10^{-5} \text{ kg/(ms)}$ was chosen.

Grid Generation

The solution outcome is strongly dependent on the grid size. More nodes improve the accuracy of a numerical solution; however, they consume more computational resources and time. Therefore, the first step in the CFD simulation was to investigate how the grid size affects the solution outcomes. Table 1 presents the effect of the grid cell number on the lift and drag coefficients at 5° and 9° angles of attack with a Reynolds number(Re) of 1.6×10^5 for the airfoils.

The results showed that a C-type grid with 76400 quadrilateral cells would be sufficient for a grid-independent solution. As certain parts required greater computational precision, the grid resolution was higher in such areas, particularly around the airfoils. The near wall cells on the upper and lower surfaces of the airfoil were adjusted to get the desired y^+ value of 1, based on boundary layer theory using the Pointwise® y^+ calculator. The inner parts of the boundary layer should be adequately resolved to a size of y^+ . The grid around the NACA 0025 airfoil and associated near-body grid are shown in Fig. 2.

Solution Methods

The steady-state convergence was also studied for a varying number of iterations, as presented in Table 2.

The study revealed that 1000 iterations were sufficient for the RANS-CFD simulations to reach a steady state. Similar steady-state convergence studies were conducted for the remaining airfoils. It was found that 1000 iterations were sufficient for this type of study. A summary of the RANS-CFD scheme used is presented in Table 3

ARTIFICIAL NEURAL NETWORK (ANN) MODEL CREATION

Artificial neural networks (ANNs) are inspired by the human brain. It can be created on a computer by simulating the processes of real neurons ([Krogh 2008](#)). ANNs ([Basheer and Hajmeer 2000](#); [Abiodun et al. 2019](#)) can learn to solve various problems. The main goal of designing an ANN model is to make good predictions for new data, or, in other words,

for the model to be generalizable. The first step in creating such a network is to create a dataset.

Dataset Preparation

The dataset used in this study includes the airfoil coordinates (X, Y), angle of attacks (α), Reynolds numbers (Re), lift coefficients (C_L), and drag coefficients (C_D). An online database for an airfoil profile generator ([Tools 2022](#)) was used to generate 201 airfoil coordinates (X, Y) for an individual airfoil. Wind turbine experimental data from ([Sheldahl and Klimas 1981](#)) were used for the remaining features, where the values of α ($0^\circ \leq \alpha \leq 180^\circ$), C_L , and C_D were obtained at different values of Re ($10^4 \leq Re \leq 10^7$) for the NACA 0012, NACA 0015, NACA 0018, NACA 0021, and NACA 0025 airfoils. Observations with an Re of 1.6×10^5 were then separated and used as test data. Eighty percentage of the remaining observations were used for training and 20% were used to validate the accuracy of the model after each epoch. Table 4 summarizes the data breakdown.

Network Architecture

The used ANN architecture, as shown in Fig. 3, consisted of an input layer, hidden layers, and an output layer, each with neurons. The input layer took all the input features, such as airfoil coordinates (X, Y), angle of attack (α), and Reynolds number (Re), and calculated the weighted sum of the inputs before adding the bias term. To generate the transformed features, this linear combination was passed through a non-linear activation function. The output of the input layer was then iteratively passed to the next layers up to the final layer, which predicted the output features, namely, the lift coefficient (C_L) and drag coefficient (C_D). Thus, through a series of mappings, the input features were mapped to the output features. Eq. 14 provides the output of a neuron in the l^{th} layer.

$$a_j^l = \sigma_l \left(\sum_{k=1}^{N^{(l-1)}} w_{jk}^l a_k^{l-1} + b_j^l \right). \quad (14)$$

The non-linear activation function in the l^{th} layer is denoted as σ_l . The weight connection

between the j^{th} neuron of the l^{th} layer and the k^{th} neuron of the $(l - 1)^{th}$ layer is represented as w_{jk} . The activation and bias terms of the j^{th} neuron in the l^{th} layer are a_j and b_j , respectively, (Nielsen 2015). A backpropagation algorithm (Rumelhart et al. 1988) was used to adjust the weights and biases. The rectified linear unit function [ReLU = max of (0, x)] has been used as a non-linear activation function, because it can train the network faster (Dubey et al. 2021).

RESULTS AND DISCUSSION

RANS-CFD approach

Simulations for various angles of attack (α) were performed to compare the results of the three turbulence models and the ANN model predictions with the experimental data (Sheldahl and Klimas 1981). Therefore, the model was solved for angles of attack (α) ranging from 0° to 30° . Here, Figs. 4a, 5a, 6a, 7a, and 8a show the simulation results of the static pressure at an angle of attack (α) 7° with three different turbulence models for the NACA 0012, NACA 0015, NACA 0018, NACA 0021, and NACA 0025 airfoils, respectively. The red and blue colors represent the maximum and minimum pressure regions, respectively. The lower surface of the leading edge exhibited the highest pressure, effectively pushing the airfoils upward, that is, normal to the incoming flow stream. The contours of the velocity components at (α) 7° angle of attack for the NACA 0012, NACA 0015, NACA 0018, NACA 0021, and NACA 0025 airfoils are also shown in Figs. 4b, 5b, 6b, 7b, and 8b, respectively. The red and blue colors represent the maximum and minimum velocity regions, respectively. The upper surface of the leading edge exhibited the highest velocity; however, it dropped at the trailing edge. The upper surface of the airfoil had a higher velocity than the lower surface.

ANN Approach

For training, five different ANN models were used. Normalization is applied to all the input features such that all the input values are within 0 - 1. An RMSprop optimizer is

used to train the weights and biases of the ANN. A learning rate (LR) of 1.0×10^{-3} is used. The models were trained for 300 epochs, with all training data fed to the network in batches of eight observations before the weights were updated using the root mean square error (RMSE) of the batch (Chai and Draxler 2014), as expressed in Eq. 15, where n is the number of observations, y_i^{real} represent the observed values, and y_i^{pred} represent the predicted values. Table 5 presents the RMSE of the models and the network architectures. Model 2, with six hidden layers and 128 nodes, performed better, and the RMSE values of C_L and C_D were 0.11632 and 0.0249, respectively. Therefore, Model 2 was used to predict the aerodynamic characteristics.

$$RMSE = \sqrt{\frac{1}{n} \sum_{i=1}^n (y_i^{real} - y_i^{pred})^2}. \quad (15)$$

RANS-CFD versus ANN

The RANS-CFD simulation results for the three different turbulence models, presented in Section 4, and the experimental data were used to compare and validate the ANN predictions. The RANS-CFD simulations and ANN predictions were performed using an angle of attack (α) ranging from 0° to 30° and a Reynolds number (Re) of 1.6×10^5 . Table 6 lists the RMSE of the turbulence models and ANN model for the NACA 0012, NACA 0015, NACA 0018, NACA 0021, and NACA 0025 airfoils.

The lift coefficient (C_L) and drag coefficient (C_D) curves for the NACA 0012, NACA 0015, NACA 0018, NACA 0021, and NACA 0025 airfoils are shown in Figs. 9, 10, 11, 12, and 13, respectively, for an angle of attack (α) in the range of 0° – -30° . The results were predicted using the ANN model, calculated using the three turbulence models, and were compared to the experimental data. In most cases, the Spalart–Allmaras and $k-\omega$ SST turbulence models performed better in calculating C_L and C_D when the angle of attack (α) was in the range of 0° – -10° . However, for α ranging from 11° to 30° , the ANN model outperformed all turbulence models for predicting the shape of the stall, whereas the turbulence models failed to do so.

CONCLUSIONS

The purpose of this study was to verify the feasibility of incorporating the knowledge of deep learning in flow analysis by developing a neural network model that can predict the aerodynamic characteristics of airfoils using experimental data. RANS-based CFD simulations with three different turbulence models in a two-dimensional domain were also performed to compare the output of the ANN model with the experimental data to verify its accuracy. Evidently, when compared with the experimental data, the ANN model easily outperformed each of the three turbulence models. More specifically, when the angle of attack (α) was in the range of 11° – 30° , the ANN model produced the most precise outcome or, in other words, had the least amount of error compared to all other turbulence models for every airfoil. Different turbulence models showed better results for different cases when α was in the range of 0° — 10° . However, even in this range of α (0° — 10°), the ANN model performed better than any other single turbulence model. Additionally, the ANN model successfully predicted the stall shape for all airfoils, whereas the turbulence models failed to do the same. However, the solution accuracy of the CFD simulations can be increased by implementing large eddy simulation (LES) or direct numerical simulation (DNS) in a three-dimensional domain at the expense of more computational power and time. Also, the accuracy of the ANN model can be improved by introducing additional data to the training dataset. Furthermore, implementing physics-informed neural networks (PINNs) can be an exciting extension of the present work. It should also be noted that the ANN model required significantly fewer computational resources than the currently used RANS-based CFD analysis. Therefore, the proposed ANN approach can be useful for accurately predicting the aerodynamic characteristics of marine rudders and other airfoil-shaped geometries. The success of our ANN model paves the way for further research on the use of deep learning in more complex flow analyses in the field of aerodynamics.

REFERENCES

Abiodun, O. I., Jantan, A., Omolara, A. E., Dada, K. V., Umar, A. M., Linus, O. U., Arshad,

- H., Kazaure, A. A., Gana, U., and Kiru, M. U. (2019). “Comprehensive review of artificial neural network applications to pattern recognition.” *IEEE Access*, 7, 158820–158846.
- Ahmed, S., Kamal, K., Ratlamwala, T. A. H., Mathavan, S., Hussain, G., Alkahtani, M., and Alsultan, M. B. M. (2022). “Aerodynamic analyses of airfoils using machine learning as an alternative to rans simulation.” *Applied Sciences*, 12(10), 5194.
- Bai, X.-D. and Zhang, W. (2022). “Machine learning for vortex induced vibration in turbulent flow.” *Computers & Fluids*, 235, 105266.
- Basheer, I. A. and Hajmeer, M. (2000). “Artificial neural networks: fundamentals, computing, design, and application.” *Journal of microbiological methods*, 43(1), 3–31.
- Bhatnagar, S., Afshar, Y., Pan, S., Duraisamy, K., and Kaushik, S. (2019). “Prediction of aerodynamic flow fields using convolutional neural networks.” *Computational Mechanics*, 64(2), 525–545.
- Bulat, M. P. and Bulat, P. V. (2013). “Comparison of turbulence models in the calculation of supersonic separated flows.” *World Applied Sciences Journal*, 27(10), 1263–1266.
- Cai, S., Mao, Z., Wang, Z., Yin, M., and Karniadakis, G. E. (2022). “Physics-informed neural networks (pinns) for fluid mechanics: A review.” *Acta Mechanica Sinica*, 1–12.
- Castelli, M. R., De Betta, S., and Benini, E. (2012). “Numerical analysis of the performance of a shrouded vertical-axis water turbine based on the naca 0025 blade profile.” *International Journal of Aerospace and Mechanical Engineering*, 6(3), 698–705.
- Chai, T. and Draxler, R. R. (2014). “Root mean square error (rmse) or mean absolute error (mae).” *Geoscientific Model Development Discussions*, 7(1), 1525–1534.
- Chen, H., He, L., Qian, W., and Wang, S. (2020). “Multiple aerodynamic coefficient prediction of airfoils using a convolutional neural network.” *Symmetry*, 12(4), 544.
- Claessens, M. (2006). “The design and testing of airfoils for application in small vertical axis wind turbines.
- Consul, C. A., Willden, R. H. J., and McIntosh, S. C. (2013). “Blockage effects on the hydrodynamic performance of a marine cross-flow turbine.” *Philosophical Transactions of the*

- Royal Society A: Mathematical, Physical and Engineering Sciences*, 371(1985), 20120299.
- Del Pino, C., Lopez-Alonso, J., Parras, L., and Fernandez-Feria, R. (2011). “Dynamics of the wing-tip vortex in the near field of a naca 0012 aerofoil.” *The Aeronautical Journal*, 115(1166), 229–239.
- Douvi, C. E., Tsavalos, I. A., and Margaris, P. D. (2012). “Evaluation of the turbulence models for the simulation of the flow over a national advisory committee for aeronautics (naca) 0012 airfoil.” *Journal of Mechanical Engineering Research*, 4(3), 100–111.
- Douvi, E. C. and Margaris, D. P. (2012). “Aerodynamic performance investigation under the influence of heavy rain of a naca 0012 airfoil for wind turbine applications.” *International Review of Mechanical Engineering*, 6(6), 1228–1235.
- Dubey, S. R., Singh, S. K., and Chaudhuri, B. B. (2021). “A comprehensive survey and performance analysis of activation functions in deep learning.” *arXiv preprint arXiv:2109.14545*.
- Frei, W. (2017). “Which turbulence model should i choose for my cfd application?” *Comsol Blog*, 1–8.
- Gao, Z., Cai, J., Li, J., Jiang, C., and Lee, C.-H. (2017). “Numerical study on mechanism of drag reduction by microblowing technique on supercritical airfoil.” *Journal of Aerospace Engineering*, 30(3), 04016084.
- Goundar, J. N., Ahmed, M. R., and Lee, Y.-H. (2012). “Numerical and experimental studies on hydrofoils for marine current turbines.” *Renewable energy*, 42, 173–179.
- Guo, C.-y., Zhang, Z.-t., Cao, X.-x., Wu, T.-c., and Su, Y.-m. (2019). “Numerical and experimental studies of hydrodynamic performance of bionic leading-edge tubercle airfoil.” *Journal of Hydrodynamics*, 31(6), 1240–1249.
- Guo, X., Li, W., and Iorio, F. (2016). “Convolutional neural networks for steady flow approximation.” *Proceedings of the 22nd ACM SIGKDD international conference on knowledge discovery and data mining*, 481–490.
- Holst, D., Church, B., Wegner, F., Pechlivanoglou, G., Nayeri, C., and Paschereit, C. (2018).

- “Experimental analysis of a naca 0021 airfoil under dynamic angle of attack variation and low reynolds numbers.” *Turbo Expo: Power for Land, Sea, and Air*, Vol. 51180, American Society of Mechanical Engineers, V009T48A010.
- Ismail, M., Wu, Z., Bakar, A., and Tariq, S. (2015). “Aerodynamic characteristics of airfoil cruise landing and high lift configurations in simulated rain environment.” *Journal of Aerospace Engineering*, 28(5), 04014131.
- Jameson, A. (1996). “The present status, challenges, and future developments in computational fluid dynamics.” *AGARD CONFERENCE PROCEEDINGS AGARD CP*, AGARD, 1–1.
- Jokar, M. and Semperlotti, F. (2021). “Finite element network analysis: A machine learning based computational framework for the simulation of physical systems.” *Computers & Structures*, 247, 106484.
- Kallstrom, K. “Exploring airfoil table generation using xfoil and overflow.
- Karim, M. M., Prasad, B., and Rahman, N. (2014). “Numerical simulation of free surface water wave for the flow around naca 0015 hydrofoil using the volume of fluid (vof) method.” *Ocean engineering*, 78, 89–94.
- Kononenko, O. and Kononenko, I. (2018). “Machine learning and finite element method for physical systems modeling.” *arXiv preprint arXiv:1801.07337*.
- Krogh, A. (2008). “What are artificial neural networks?” *Nature biotechnology*, 26(2), 195–197.
- Lee, S. and You, D. (2019). “Data-driven prediction of unsteady flow over a circular cylinder using deep learning.” *Journal of Fluid Mechanics*, 879, 217–254.
- Lin, Y., Lam, K., Zou, L., and Liu, Y. (2013). “Numerical study of flows past airfoils with wavy surfaces.” *Journal of fluids and structures*, 36, 136–148.
- Liu, J., Quadvlieg, F., and Hekkenberg, R. (2016). “Impacts of the rudder profile on manoeuvring performance of ships.” *Ocean Engineering*, 124, 226–240.
- Liu, W., Wang, Z., Liu, X., Zeng, N., Liu, Y., and Alsaadi, F. E. (2017). “A survey of deep

- neural network architectures and their applications.” *Neurocomputing*, 234, 11–26.
- Mao, Z., Jagtap, A. D., and Karniadakis, G. E. (2020). “Physics-informed neural networks for high-speed flows.” *Computer Methods in Applied Mechanics and Engineering*, 360, 112789.
- Menter, F. R. (1994). “Two-equation eddy-viscosity turbulence models for engineering applications.” *AIAA journal*, 32(8), 1598–1605.
- Mohamed, M. (2012). “Performance investigation of h-rotor darrieus turbine with new airfoil shapes.” *Energy*, 47(1), 522–530.
- Nielsen, M. A. (2015). *Neural networks and deep learning*, Vol. 25. Determination press San Francisco, CA, USA.
- Oztiryaki, F. G. and Piskin, T. (2021). “Airfoil performance analysis using shallow neural networks.” *AIAA Scitech 2021 Forum*, 0174.
- Peng, W., Zhang, Y., Laurendeau, E., and Desmarais, M. C. (2022). “Learning aerodynamics with neural network.” *Scientific Reports*, 12(1), 1–10.
- Raissi, M., Perdikaris, P., and Karniadakis, G. E. (2019). “Physics-informed neural networks: A deep learning framework for solving forward and inverse problems involving nonlinear partial differential equations.” *Journal of Computational physics*, 378, 686–707.
- Ram, B. R. R., Surendran, S., and Lee, S. (2015). “Computer and experimental simulations on the fin effect on ship resistance.” *Ships and Offshore Structures*, 10(2), 122–131.
- Raman, R. K., Dewang, Y., and Raghuwanshi, J. (2018). “A review on applications of computational fluid dynamics.” *International Journal of LNCT*, 2(6), 137–143.
- Rojas-Sola, J. I., García-Baena, C., and Hermoso-Orzáez, M. J. (2016). “A review of the computational fluid dynamics simulation software: Advantages, disadvantages and main applications.” *Journal of Magnetohydrodynamics and Plasma Research*, 21(4), 417–424.
- Rumelhart, D. E., Hinton, G. E., and Williams, R. J. (1988). “Neurocomputing: Foundations of research.
- Şahin, İ. and Acir, A. (2015). “Numerical and experimental investigations of lift and drag performances of naca 0015 wind turbine airfoil.” *International Journal of Materials, Me-*

- chanics and Manufacturing*, 3(1), 22–25.
- Sekar, V., Jiang, Q., Shu, C., and Khoo, B. C. (2019). “Fast flow field prediction over airfoils using deep learning approach.” *Physics of Fluids*, 31(5), 057103.
- Sekar, V., Jiang, Q., Shu, C., and Khoo, B. C. (2022). “Accurate near wall steady flow field prediction using physics informed neural network (pinn).” *arXiv preprint arXiv:2204.03352*.
- Sener, M. Z. and Aksu, E. (2022). “The numerical investigation of the rotation speed and reynolds number variations of a naca 0012 airfoil.” *Ocean Engineering*, 249, 110899.
- Sheldahl, R. E. and Klimas, P. C. (1981). “Aerodynamic characteristics of seven symmetrical airfoil sections through 180-degree angle of attack for use in aerodynamic analysis of vertical axis wind turbines.” *Report no.*, Sandia National Labs., Albuquerque, NM (USA).
- Shih, T.-H., Liou, W. W., Shabbir, A., Yang, Z., and Zhu, J. (1995). “A new k- ϵ eddy viscosity model for high reynolds number turbulent flows.” *Computers & fluids*, 24(3), 227–238.
- Singh, S. K., Garg, M., Narayanan, S., Ayton, L., and Chaitanya, P. (2022). “On the reductions of airfoil broadband noise through sinusoidal trailing-edge serrations.” *Journal of Aerospace Engineering*, 35(2), 04022003.
- Spalart, P. and Allmaras, S. (1992). “A one-equation turbulence model for aerodynamic flows.” *30th aerospace sciences meeting and exhibit*, 439.
- Suvanjumrat, C. (2017). “Comparison of turbulence models for flow past naca0015 airfoil using openfoam.” *Engineering Journal*, 21, 207–221.
- Takekoshi, Y., Kawamura, T., Yamaguchi, H., Maeda, M., Ishii, N., Kimura, K., Take-tani, T., and Fujii, A. (2005). “Study on the design of propeller blade sections using the optimization algorithm.” *Journal of marine science and technology*, 10(2), 70–81.
- Tang, C., Gee, K., and Lawrence, S. (2005). “Generation of aerodynamic data using a design of experiment and data fusion approach.” *43rd AIAA Aerospace Sciences Meeting and Exhibit*, 1137.

- Tasif, T. H., Rahman, M. H., Fazle, A. B., and Karim, M. M. (2017). “Numerical prediction of flow past a marine rudder.” *Procedia engineering*, 194, 59–66.
- Thirumalainambi, R. and Bardina, J. (2003). “Training data requirement for a neural network to predict aerodynamic coefficients.” *Independent component analyses, wavelets, and neural networks*, Vol. 5102, SPIE, 92–103.
- Timmer, W. (2008). “Two-dimensional low-reynolds number wind tunnel results for airfoil naca 0018.” *Wind engineering*, 32(6), 525–537.
- Tools, A. (2022). “Airfoil tools.
- Versteeg, H. K. and Malalasekera, W. (2007). *An introduction to computational fluid dynamics: the finite volume method*. Pearson education.
- Xu, M., Cheng, H., and Ji, B. (2021). “Rans simulation of unsteady cavitation around a clark-y hydrofoil with the assistance of machine learning.” *Ocean Engineering*, 231, 109058.
- Yilmaz, S., Erdem, D., and Kavsaoglu, M. (2013). “Effects of duct shape on a ducted propeller performance.” *51st AIAA aerospace sciences meeting including the new horizons forum and aerospace exposition*, 803.
- Yu, B., Xie, L., and Wang, F. (2019). “An improved deep convolutional neural network to predict airfoil lift coefficient.” *International Conference on Aerospace System Science and Engineering*, Springer, 275–286.
- Yuan, Z., Wang, Y., Qiu, Y., Bai, J., and Chen, G. (2018). “Aerodynamic coefficient prediction of airfoils with convolutional neural network.” *Asia-Pacific International Symposium on Aerospace Technology*, Springer, 34–46.
- Zhang, Y., Sung, W. J., and Mavris, D. N. (2018). “Application of convolutional neural network to predict airfoil lift coefficient.” *2018 AIAA/ASCE/AHS/ASC structures, structural dynamics, and materials conference*, 1903.

List of Tables

1	Grid convergence study for a different number of cells on the surface of airfoils with a Reynolds number of 1.6×10^5	20
2	Steady state convergence study for a different number of iterations on the NACA 0025 airfoil with a Reynolds number of 1.6×10^5	21
3	Summary of the RANS-CFD scheme used.	22
4	Partition of the dataset.	23
5	ANN performance for five different models.	24
6	RMSE of the turbulence models and ANN model	25

TABLE 1. Grid convergence study for a different number of cells on the surface of airfoils with a Reynolds number of 1.6×10^5

Airfoils	Test case	No. of cells	Angle of attack, α							
			5°				9°			
			C_L	% Deviation from case 1	C_D	% Deviation from case 1	C_L	% Deviation from case 1	C_D	% Deviation from case 1
NACA 0012	Case 3	35000	0.45019	-11.83%	0.018369	18.86%	0.89134	7.04%	0.026606	-9.46%
	Case 2	54000	0.50976	-0.16%	0.016181	4.70%	0.86573	3.97%	0.027576	-6.15%
	Case 1	76400	0.51059	0.00%	0.015454	0.00%	0.83269	0.00%	0.029385	0.00%
	Case 4	110000	0.51011	-0.09%	0.01548	0.17%	0.83805	0.64%	0.029173	-0.72%
NACA 0015	Case 3	35000	0.48989	1.87%	0.019548	2.39%	0.85539	2.88%	0.027152	3.07%
	Case 2	54000	0.48982	1.85%	0.019335	1.27%	0.84022	1.05%	0.027127	2.98%
	Case 1	76400	0.4809	0.00%	0.019092	0.00%	0.83144	0.00%	0.026342	0.00%
	Case 4	110000	0.48225	0.28%	0.019086	-0.03%	0.83414	0.32%	0.026583	0.91%
NACA 0018	Case 3	35000	0.46223	7.42%	0.021058	6.21%	0.8093	4.12%	0.028901	3.74%
	Case 2	54000	0.44358	3.08%	0.0200838	1.29%	0.79636	2.46%	0.028595	2.64%
	Case 1	76400	0.43031	0.00%	0.019827	0.00%	0.77725	0.00%	0.027858	0.00%
	Case 4	110000	0.43131	0.23%	0.019665	-0.82%	0.78167	0.57%	0.027634	-0.80%
NACA 0021	Case 3	35000	0.42687	-10.17%	0.026925	-11.63%	0.7548	11.96%	0.031659	9.69%
	Case 2	54000	0.45131	-5.02%	0.02958	-2.92%	0.70565	4.67%	0.030534	5.79%
	Case 1	76400	0.47518	0.00%	0.03047	0.00%	0.67416	0.00%	0.028862	0.00%
	Case 4	110000	0.47901	0.81%	0.030195	-0.90%	0.68318	1.34%	0.029349	1.69%
NACA 0025	Case 3	35000	0.3084	18.35%	0.026202	6.72%	0.64883	16.31%	0.036877	10.66%
	Case 2	54000	0.28713	10.19%	0.025104	2.25%	0.59685	6.99%	0.035774	7.35%
	Case 1	76400	0.26058	0.00%	0.024552	0.00%	0.55786	0.00%	0.033324	0.00%
	Case 4	110000	0.26173	0.44%	0.024693	0.57%	0.55059	-1.30%	0.033297	-0.08%

TABLE 2. Steady state convergence study for a different number of iterations on the NACA 0025 airfoil with a Reynolds number of 1.6×10^5

Test case	No. of iterations	Angle of attack, α			
		9°			
		C_L	% Deviation from case 1	C_D	% Deviation from case 1
Case 3	100	0.90016	63.49%	0.70451	2015.83%
Case 2	500	0.58186	5.68%	0.04072	22.30%
Case 1	1000	0.55059	0.00%	0.033297	0.00%
Case 4	1300	0.54932	-0.23%	0.03325	-0.14%
Case 5	1500	0.54938	-0.22%	0.03341	0.33%

TABLE 3. Summary of the RANS-CFD scheme used.

Particulars	Scheme
Solver	2D double-precision parallel steady-state
Pressure–Velocity Coupling	SIMPLE
Gradient	Least-Square Cell-Based
Pressure	Second Order
Momentum	Second Order
Turbulent Kinetic Energy	Second Order
Specific Dissipation Rate	Second-Order Upwind
Convergence Criteria	10^{-6}
Iteration	1000

TABLE 4. Partition of the dataset.

Dataset	Observations
Training data	2078
Validation data	520
Testing data	80

TABLE 5. ANN performance for five different models.

ANN model	No. of hidden layers	No. of nodes	RMSE	
			C_L	C_D
Model 1	6	80	0.12239	0.03768
Model 2	6	128	0.11632	0.02490
Model 3	5	64	0.14085	0.04243
Model 4	6	256	0.13325	0.02966
Model 5	5	256	0.14139	0.03376

TABLE 6. RMSE of the turbulence models and ANN model

Airfoil	Range (α)	k- ϵ Realizable		k- ω SST		Spalart–Allmaras		ANN	
		C_L	C_D	C_L	C_D	C_L	C_D	C_L	C_D
NACA 0012	0 - 10	0.05323	0.01799	0.03140	0.00422	0.02659	0.00520	0.10566	0.00832
	11 - 20	0.64753	0.05631	0.71721	0.04382	0.68629	0.06883	0.04295	0.01148
	21 - 30	0.10053	0.03412	0.09353	0.02776	0.10369	0.01864	0.03798	0.00349
NACA 0015	0 - 10	0.07283	0.01806	0.04261	0.00476	0.02887	0.00530	0.12331	0.01904
	11 - 20	0.42116	0.05578	0.49072	0.05153	0.62202	0.06662	0.03413	0.02830
	21 - 30	0.44319	0.05382	0.40096	0.03727	0.29646	0.03702	0.02874	0.00289
NACA 0018	0 - 10	0.07331	0.01860	0.04188	0.00506	0.02905	0.00567	0.03629	0.01169
	11 - 20	0.14517	0.03971	0.25118	0.04571	0.36821	0.05054	0.02201	0.01938
	21 - 30	0.23157	0.05923	0.32460	0.05840	0.30054	0.07503	0.02632	0.00561
NACA 0021	0 - 10	0.08491	0.02122	0.07987	0.00821	0.06673	0.00740	0.18676	0.01736
	11 - 20	0.14978	0.04469	0.20955	0.04067	0.24095	0.04095	0.13447	0.03906
	21 - 30	0.26715	0.12035	0.32603	0.11694	0.38560	0.10108	0.11808	0.00376
NACA 0025	0 - 10	0.06083	0.02441	0.09290	0.00716	0.05917	0.00673	0.11846	0.00538
	11 - 20	0.10247	0.04679	0.09231	0.03228	0.11329	0.03196	0.07263	0.00268
	21 - 30	0.29518	0.13438	0.24032	0.18745	0.16898	0.23775	0.07442	0.03827

List of Figures

1	Flow past an airfoil simulation in the C-type domain.	28
2	(a) Grid around NACA 0025 airfoil and (b) Detail close to the NACA 0025 airfoil.	29
3	ANN architecture used in the aerodynamic characteristic prediction network.	30
4	(a) Pressure and (b) velocity contours of the NACA 0012 airfoil at 7° angle of attack (α) with a Reynolds number (Re) of 1.6×10^5 using three turbulence models.	31
5	(a) Pressure and (b) velocity contours of the NACA 0015 airfoil at 7° angle of attack (α) with a Reynolds number (Re) of 1.6×10^5 using three turbulence models.	32
6	(a) Pressure and (b) velocity contours of the NACA 0018 airfoil at 7° angle of attack (α) with a Reynolds number (Re) of 1.6×10^5 using three turbulence models.	33
7	(a) Pressure and (b) velocity contours of the NACA 0021 airfoil at 7° angle of attack (α) with a Reynolds number (Re) of 1.6×10^5 using three turbulence models.	34
8	(a) Pressure and (b) velocity contours of the NACA 0025 airfoil at 7° angle of attack (α) with a Reynolds number (Re) of 1.6×10^5 using three turbulence models.	35
9	Result comparisons of the NACA 0012 with a Reynolds number (Re) of 1.6×10^5 for (a) lift coefficient (C_L) and (b) drag coefficient (C_D).	36
10	Result comparisons of the NACA 0015 with a Reynolds number (Re) of 1.6×10^5 for (a) lift coefficient (C_L) and (b) drag coefficient (C_D).	37
11	Result comparisons of the NACA 0018 with a Reynolds number (Re) of 1.6×10^5 for (a) lift coefficient (C_L) and (b) drag coefficient (C_D).	38

12	Result comparisons of the NACA 0021 with a Reynolds number (Re) of 1.6×10^5 for (a) lift coefficient (C_L) and (b) drag coefficient (C_D).	39
13	Result comparisons of the NACA 0025 with a Reynolds number (Re) of 1.6×10^5 for (a) lift coefficient (C_L) and (b) drag coefficient (C_D).	40

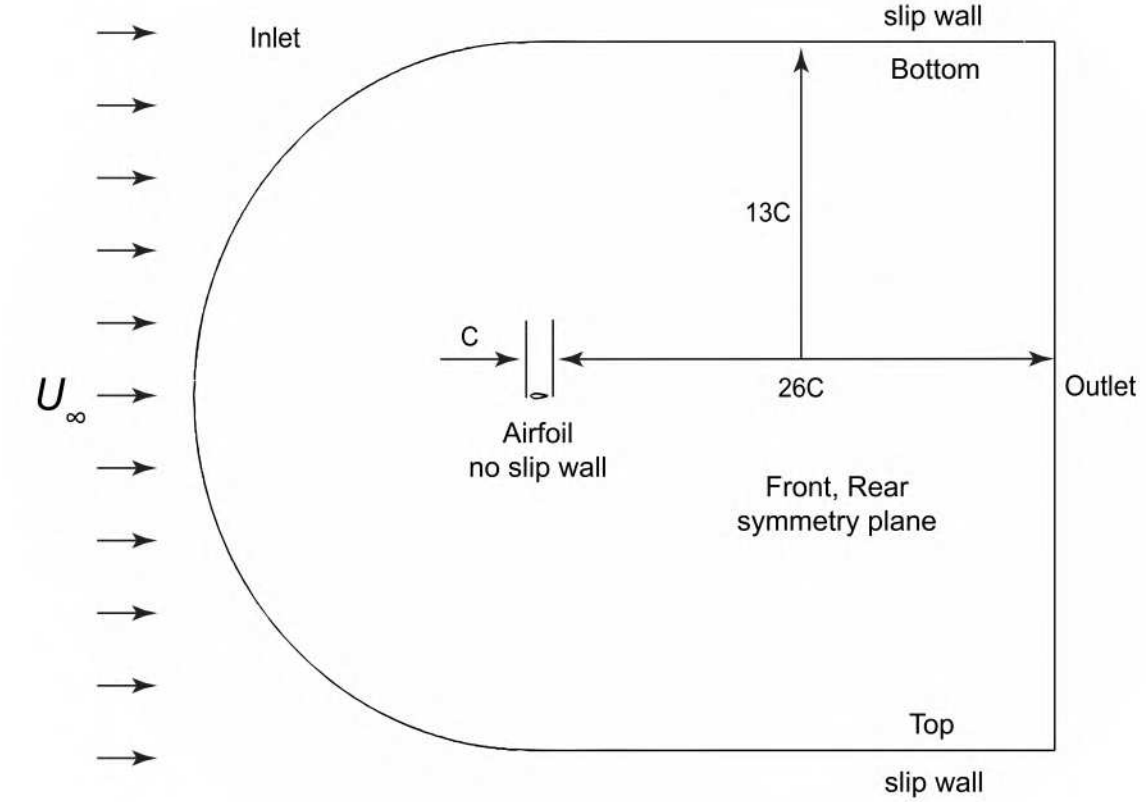
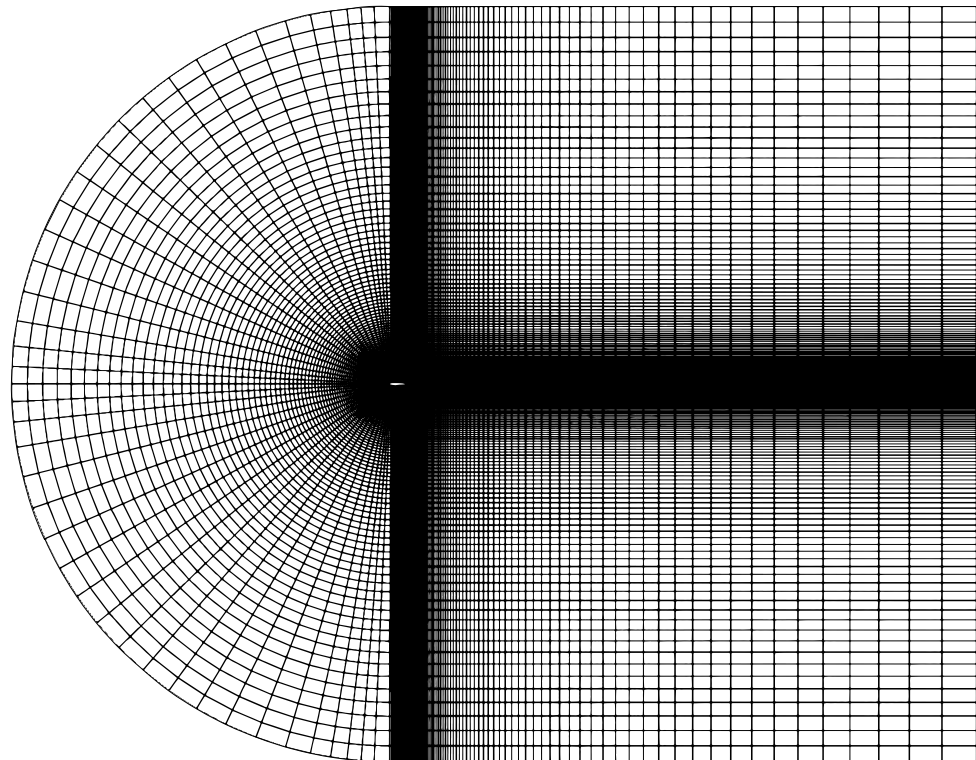
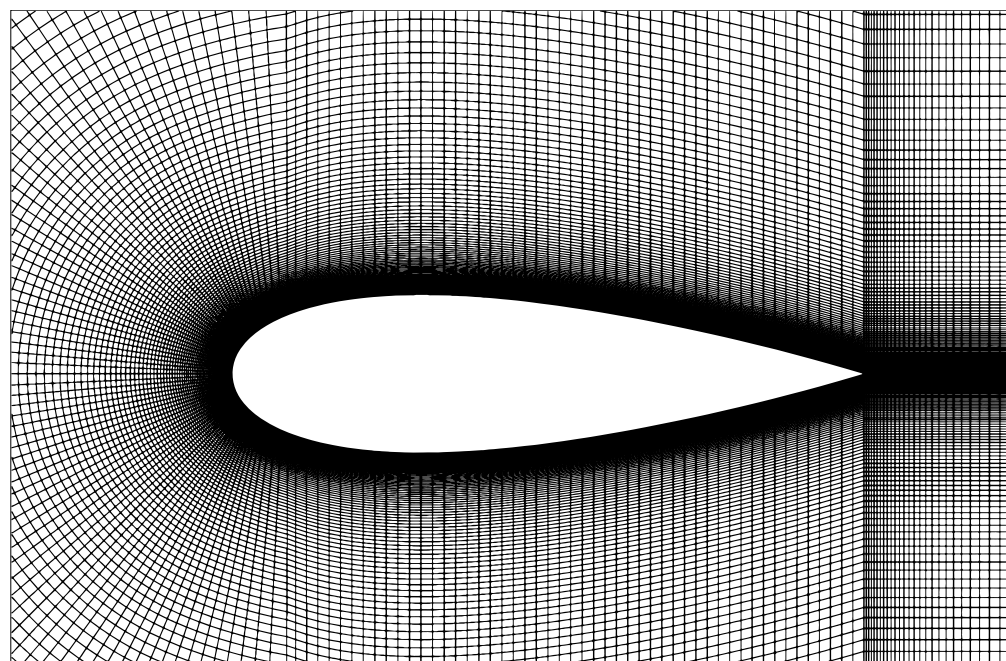


Fig. 1. Flow past an airfoil simulation in the C-type domain.



(a)



(b)

Fig. 2. (a) Grid around NACA 0025 airfoil and (b) Detail close to the NACA 0025 airfoil.

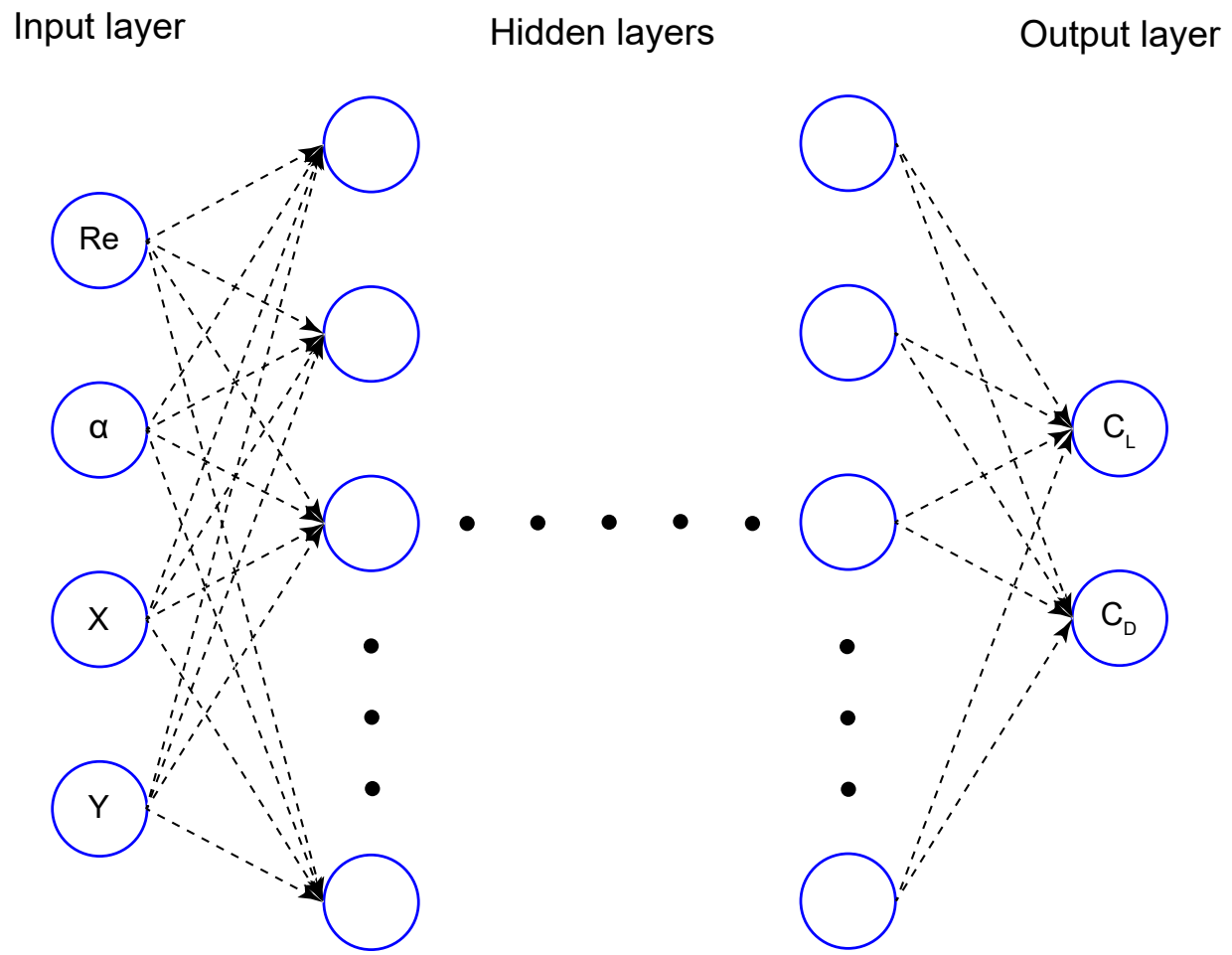
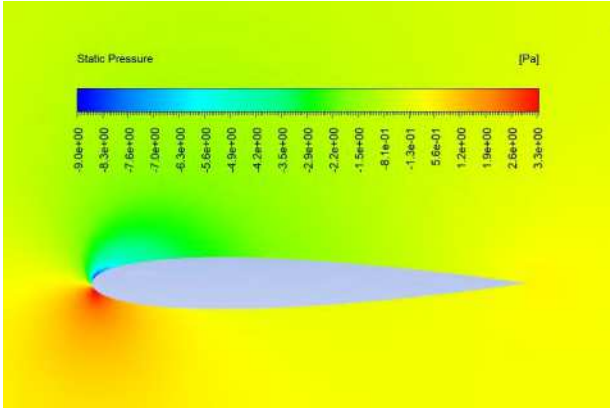
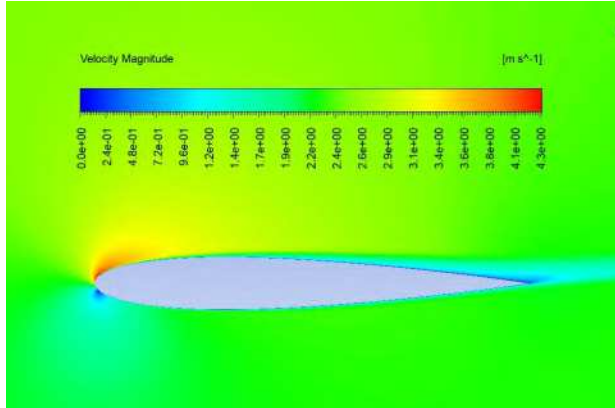


Fig. 3. ANN architecture used in the aerodynamic characteristic prediction network.

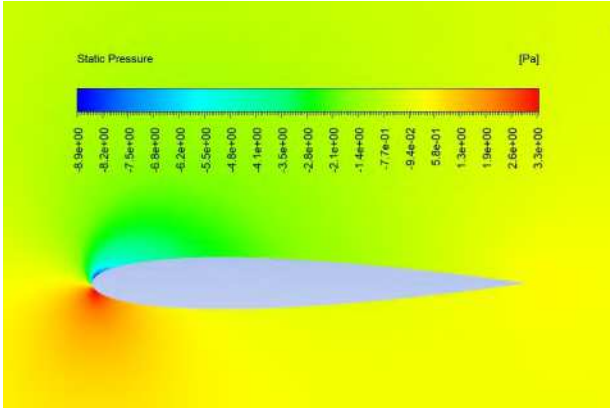
Spalart-Allmaras



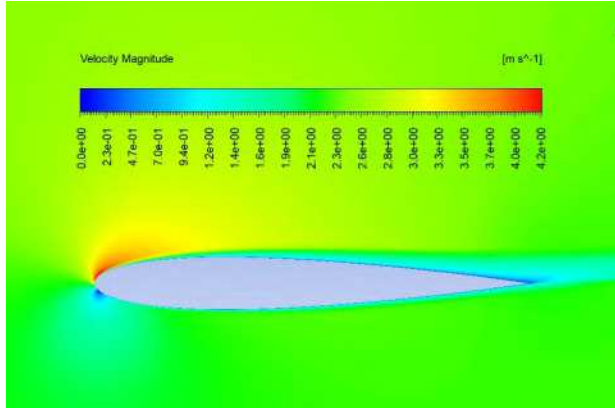
Spalart-Allmaras



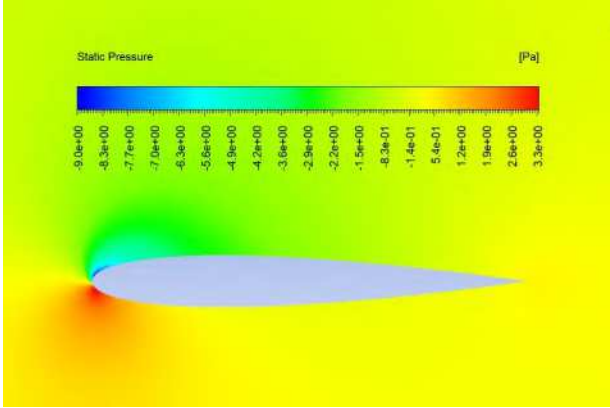
$k-\epsilon$ Realizable



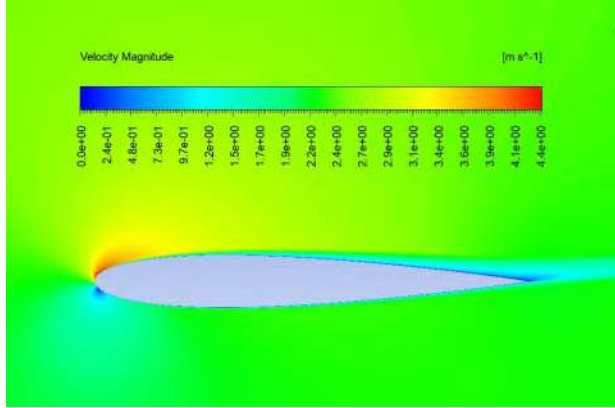
$k-\epsilon$ Realizable



$k-\omega$ SST



$k-\omega$ SST



(a)

(b)

Fig. 4. (a) Pressure and (b) velocity contours of the NACA 0012 airfoil at 7° angle of attack (α) with a Reynolds number (Re) of 1.6×10^5 using three turbulence models.

Spalart–Allmaras

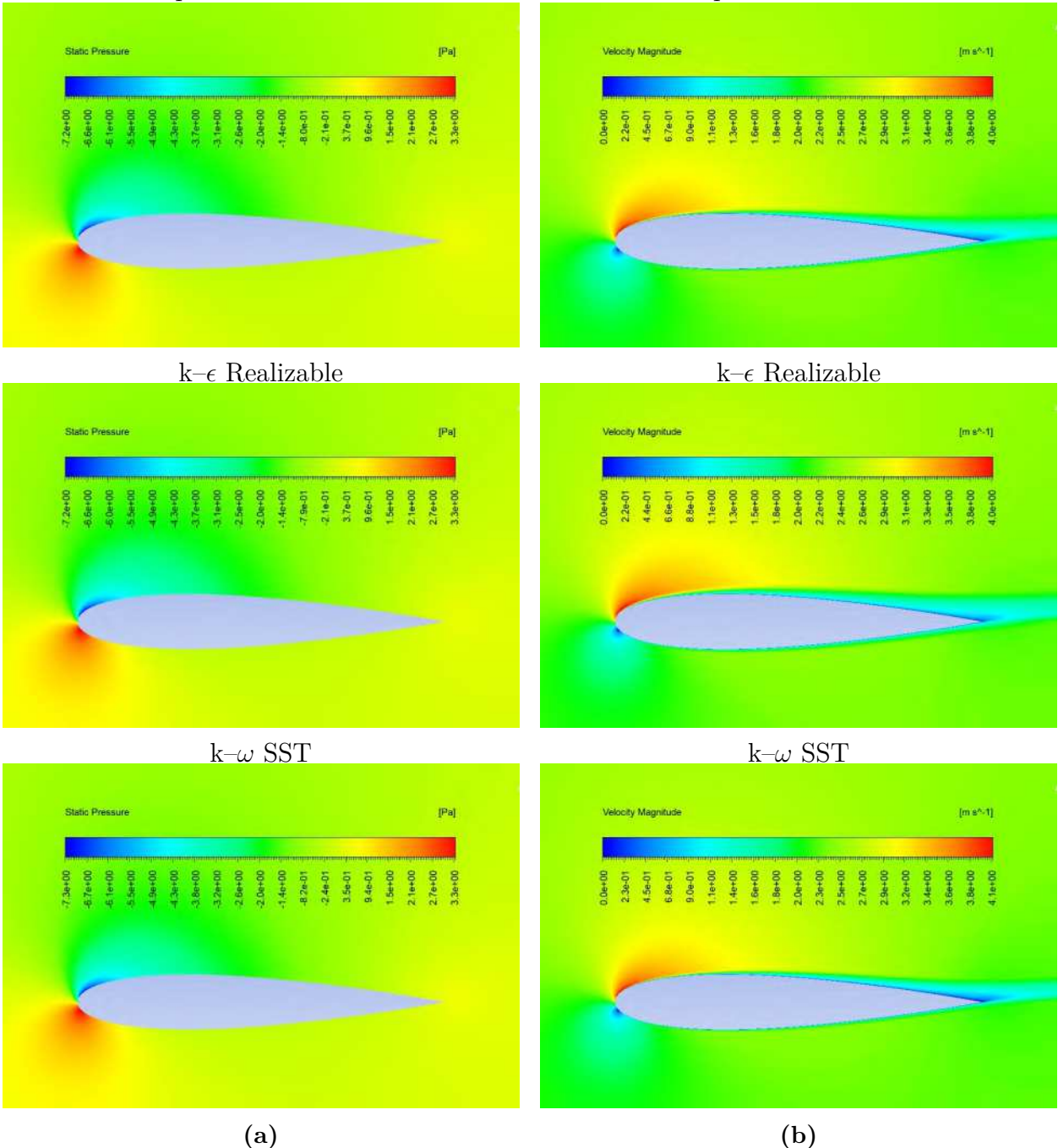


Fig. 5. (a) Pressure and (b) velocity contours of the NACA 0015 airfoil at 7° angle of attack (α) with a Reynolds number (Re) of 1.6×10^5 using three turbulence models.

Spalart–Allmaras

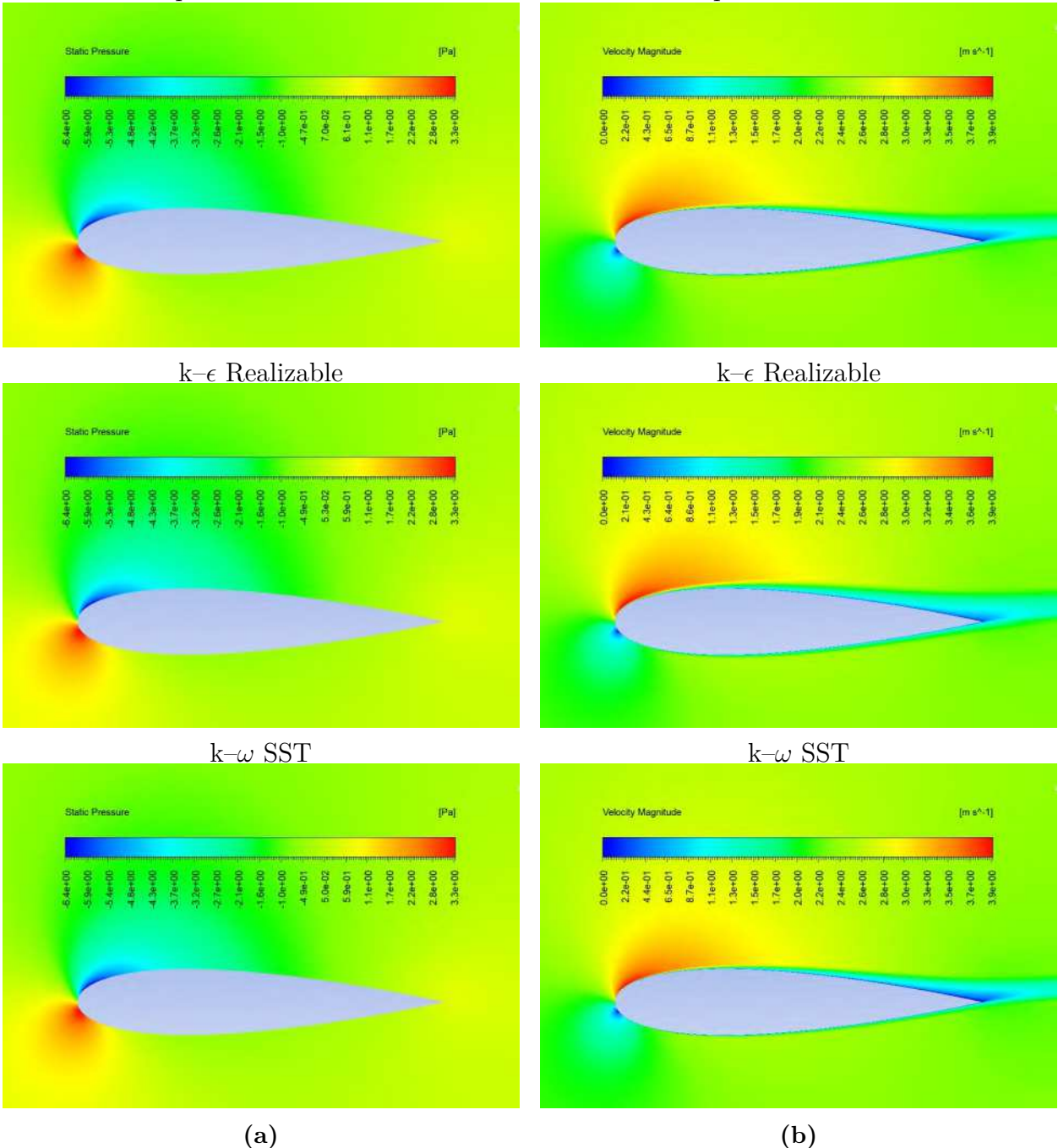


Fig. 6. (a) Pressure and (b) velocity contours of the NACA 0018 airfoil at 7° angle of attack (α) with a Reynolds number (Re) of 1.6×10^5 using three turbulence models.

Spalart–Allmaras

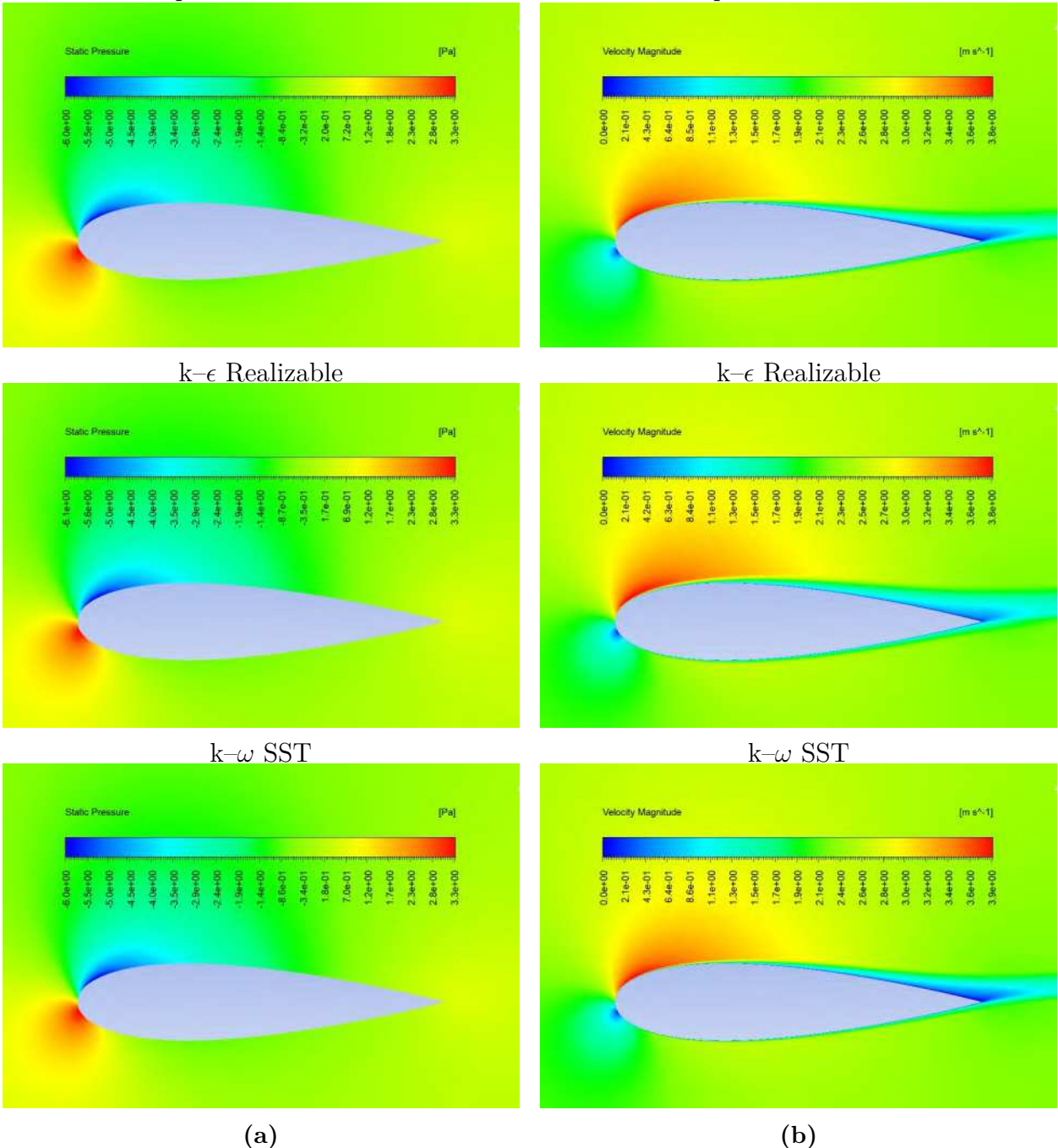


Fig. 7. (a) Pressure and (b) velocity contours of the NACA 0021 airfoil at 7° angle of attack (α) with a Reynolds number (Re) of 1.6×10^5 using three turbulence models.

Spalart–Allmaras

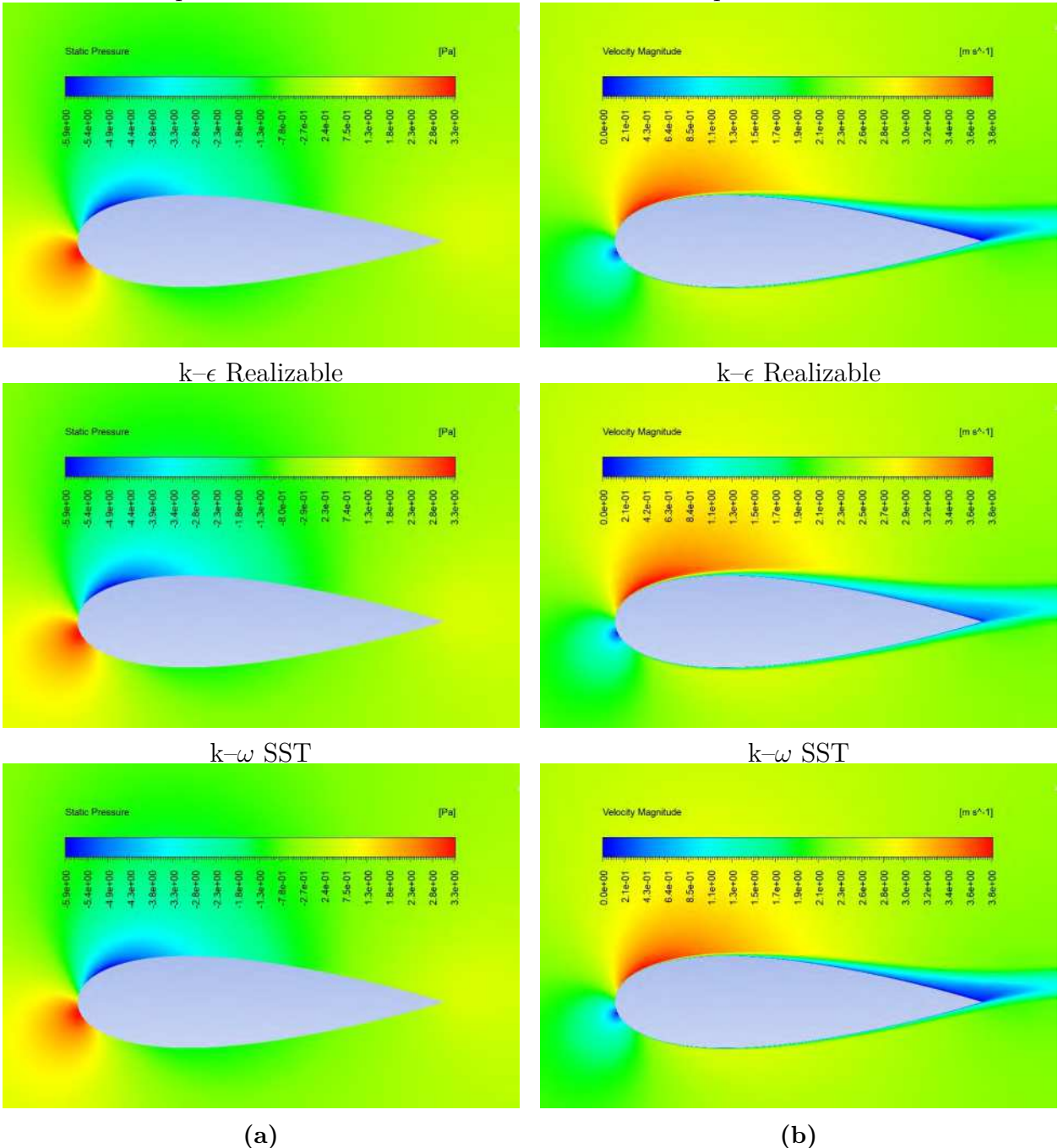
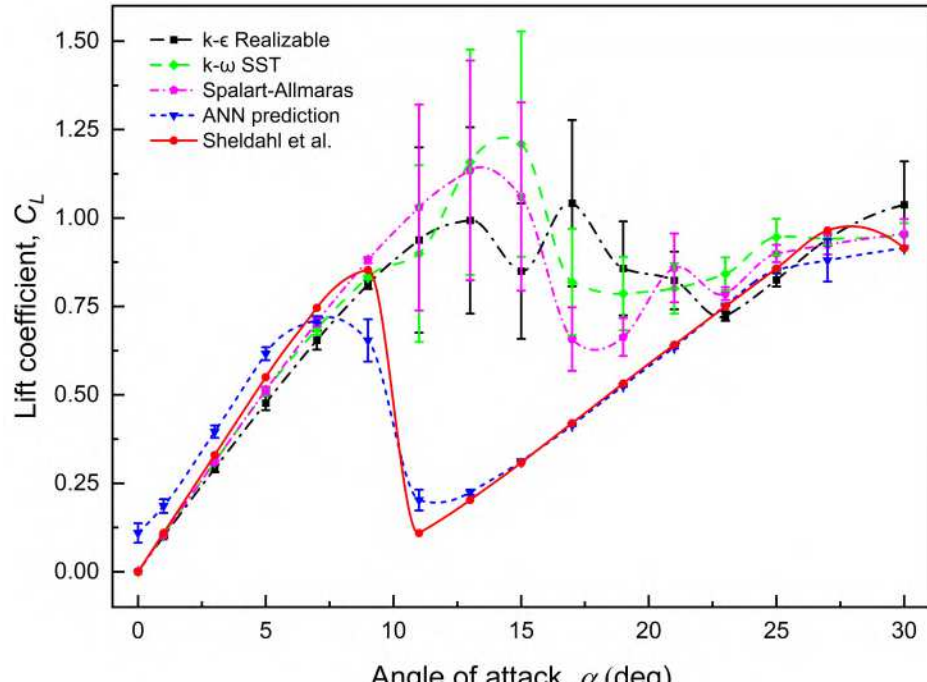
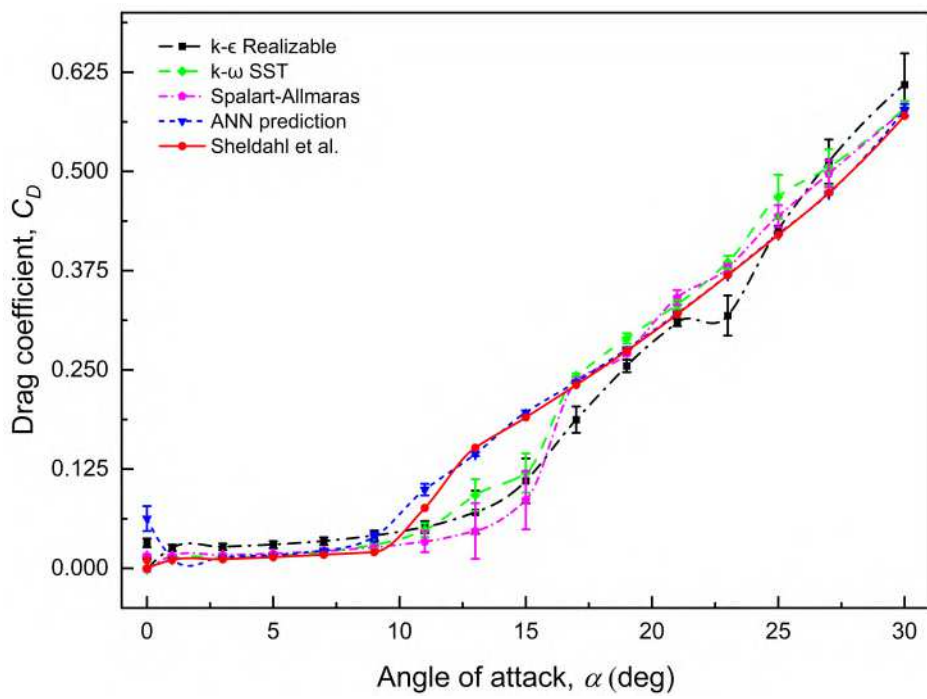


Fig. 8. (a) Pressure and (b) velocity contours of the NACA 0025 airfoil at 7° angle of attack (α) with a Reynolds number (Re) of 1.6×10^5 using three turbulence models.

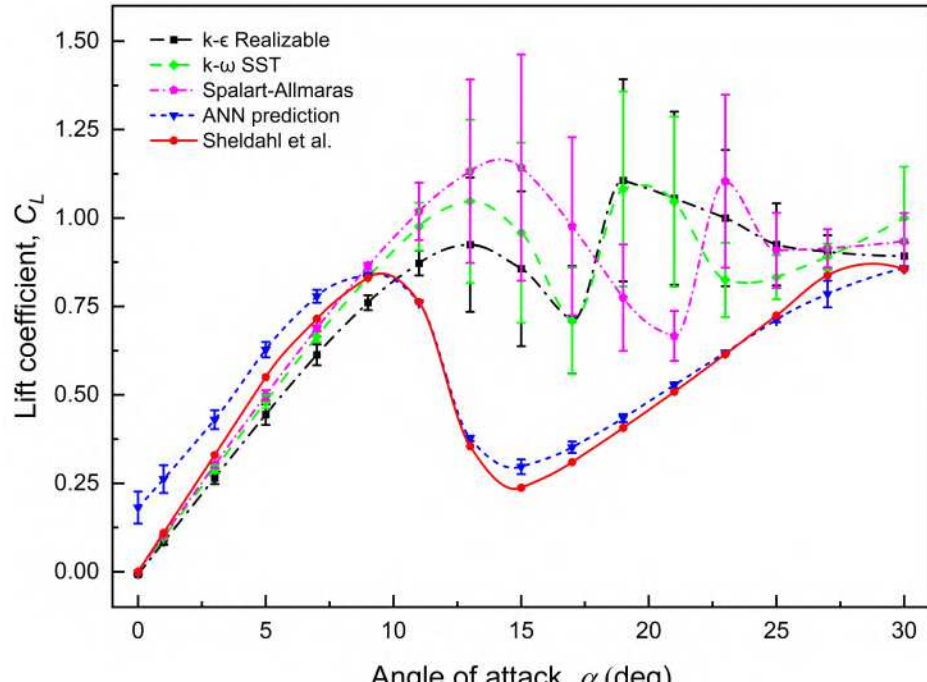


(a)

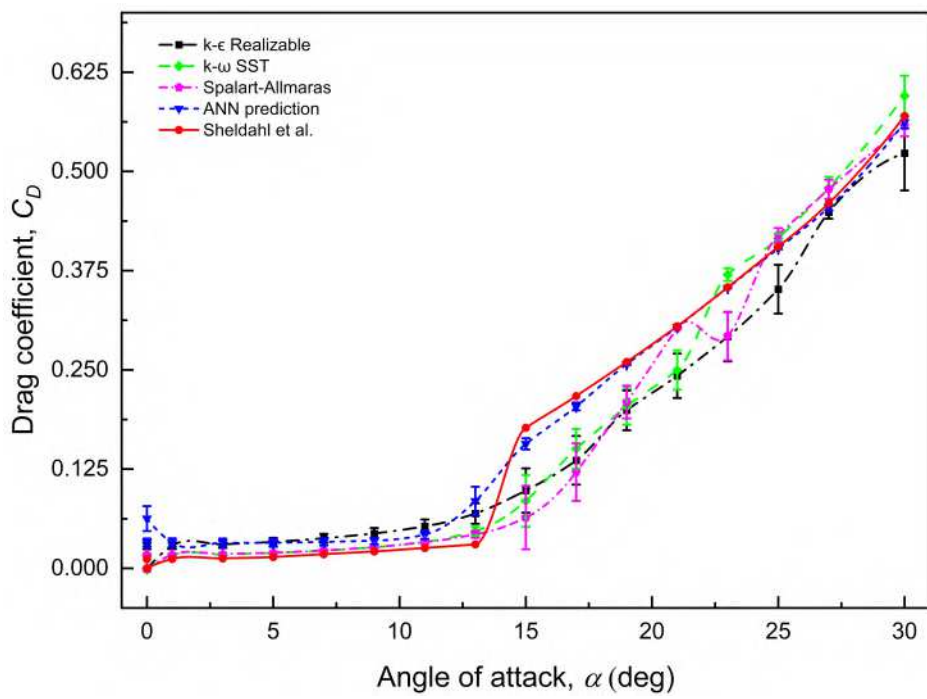


(b)

Fig. 9. Result comparisons of the NACA 0012 with a Reynolds number (Re) of 1.6×10^5 for (a) lift coefficient (C_L) and (b) drag coefficient (C_D).

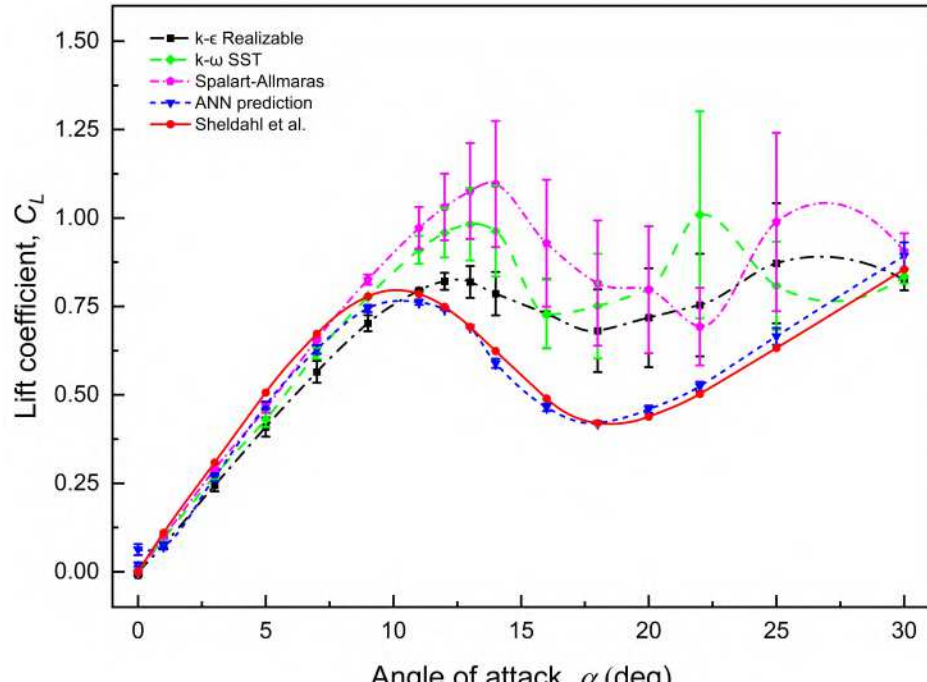


(a)

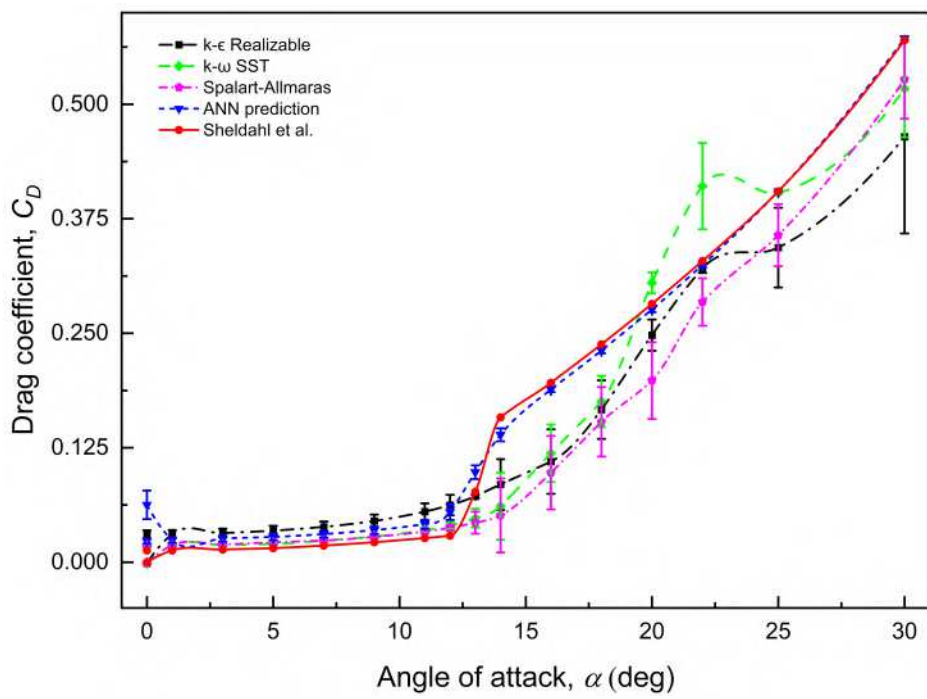


(b)

Fig. 10. Result comparisons of the NACA 0015 with a Reynolds number (Re) of 1.6×10^5 for (a) lift coefficient (C_L) and (b) drag coefficient (C_D).

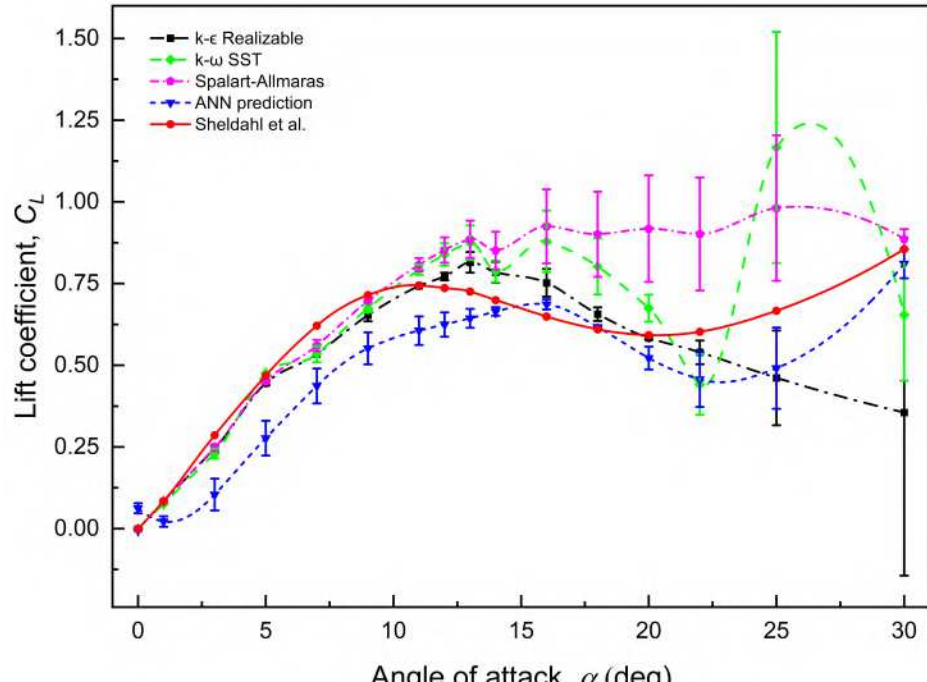


(a)

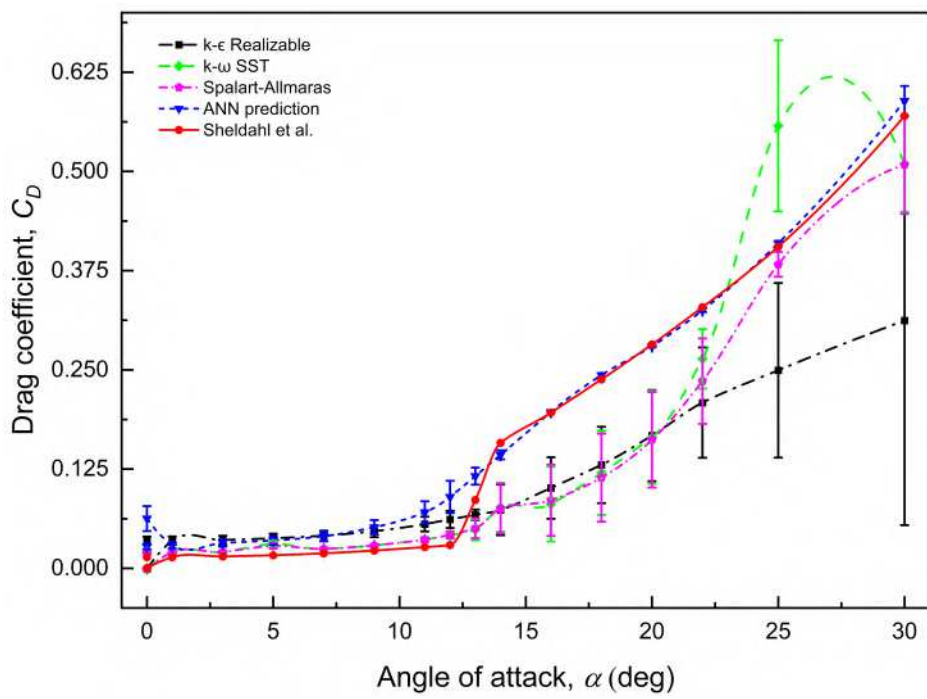


(b)

Fig. 11. Result comparisons of the NACA 0018 with a Reynolds number (Re) of 1.6×10^5 for (a) lift coefficient (C_L) and (b) drag coefficient (C_D).

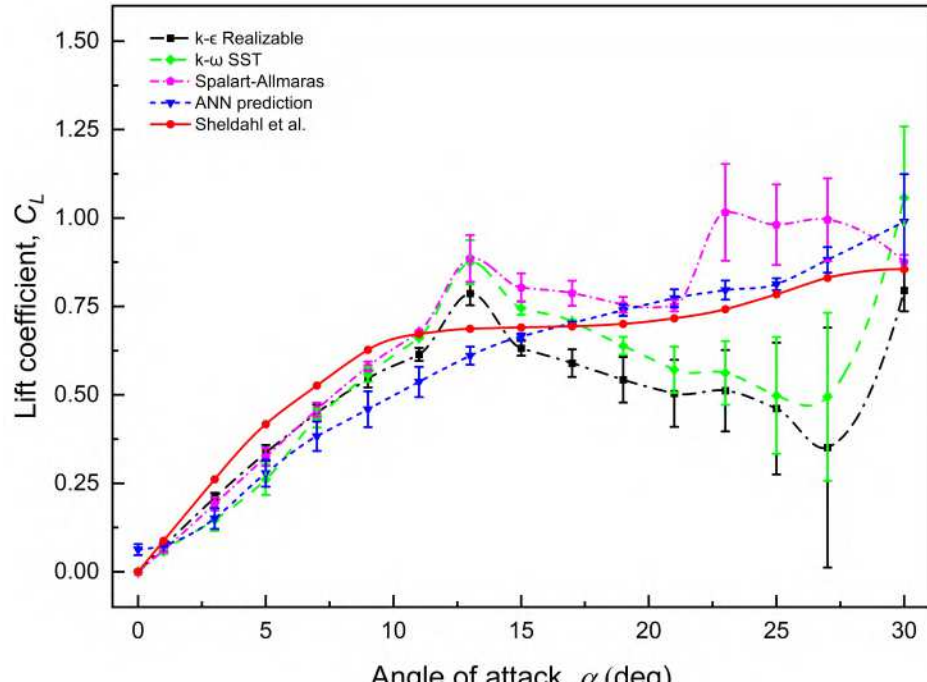


(a)

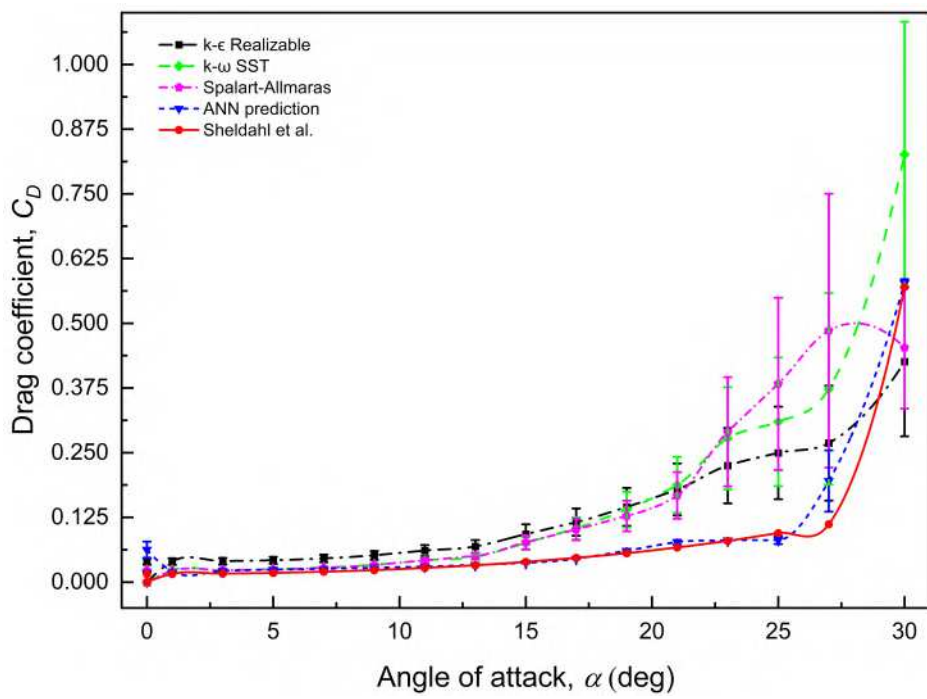


(b)

Fig. 12. Result comparisons of the NACA 0021 with a Reynolds number (Re) of 1.6×10^5 for (a) lift coefficient (C_L) and (b) drag coefficient (C_D).



(a)



(b)

Fig. 13. Result comparisons of the NACA 0025 with a Reynolds number (Re) of 1.6×10^5 for (a) lift coefficient (C_L) and (b) drag coefficient (C_D).